Journal of Applied Sciences and Nanotechnology

Journal homepage: jasn.uotechnology.edu.iq

Surface-Enhanced Raman Scattering Sensors: A Comparative Study of Copper and Palladium Nanostructures for Nitrite Detection

[1]Intisar A. Naseef [*], [2]Alwan M. Alwan, [2]Mehdi Q. Zayer, [3]Layla A. Wali

[1]Materials research directorate, Ministry of Science and Technology, Bagdad- Iraq
[2]Department of Applied Sciences, University of Technology, Baghdad-Iraq
[3]College of Basic Education, University of Al-Mustansiriyah, Baghdad- Iraq

A R T I C L E I N F O

Article history:
Received: April, 23, 2024
Accepted: August, 16, 2024
Available online: September, 10, 2024

Keywords:
Plasmons,
CuNWs,
PdNPs,
SERS sensors,
$NaNO_2$ detection

Corresponding Author:
Alwan M. Alwan
alkrzsm@yahoo.com

A B S T R A C T

In scientific research, the search for cost-efficient and scalable functional materials for substantial and practical applications is necessary. Therefore, metallic materials at the nanoscale represent a rapidly growing area of research, especially as plasmonic materials in the field of surface-enhanced Raman scattering (SERS). In this study, the potential of copper nanowires (CuNWs) and palladium nanoparticles (PdNPs) as thin films on the porous silicon (PS) surface was investigated and compared. Their parameters as plasmonic SERS sensing materials were investigated by detecting sodium nitrite ($NaNO_2$) molecules as the analyzing material. CuNWs and PdNPs were locally deposited on the PS substrate by the immersion method to synthesize Cu/PS and Pd/PS SERS sensors. The successful fabrication of these sensors was confirmed by X-ray diffraction (XRD), energy dispersive X-ray spectroscopy (EDS), field emission scanning electron microscopy (FESEM), and Raman measurements. The results show that the nanostructures of the metallic thin films are evenly distributed on the PS surface and that hot spot areas have formed in between. The Raman peaks of $NaNO_2$ were effectively detected even at extremely low concentration values. Therefore, CuNWs and PdNPs were integrated with PS in the SERS to improve the detection process. Excellent detection of (5×10^{-6}) M $NaNO_2$ concentration was achieved with the Cu/PS and Pd/PS SERS sensors with high amplification factors of (0.43×10^{8}) and (0.11×10^{8}), respectively.

https://doi.org/10.53293/jasn.2024.7357.1290, Department of Applied Sciences, University of Technology - Iraq.

1. Introduction

The sensor's scheme's design and fabrication encompass a specific exploration of materials with preferred transducer features. Nanostructured materials have garnered considerable attention due to their distinctive physiochemical features, including high surface-to-volume ratio, small size, light absorption, optical sensitivity, and electrical and thermal conductivity [1, 2]. Plasmonic nanostructured materials are engineered to manipulate and control visible wavelengths at a nanometer scale, offering significant potential for effective impact in applications such as photonic interconnects and sensitive analytical devices [3]. Surface plasmons represent a

physiochemical phenomenon involving the collective oscillations and coherent plasma oscillations of free electrons induced by an electromagnetic (EM) field and observed on the surfaces of nanostructures or noble metal thin films. Plasmons investigate how light interacts with metallic nanostructures at the metal-dielectric interface [3, 4]. The adjustments and chemical modifications applied to the surface of plasmon resonance (SPR) features are crucial for designing improved active substrates, for example, porous silicon (PS), the complex matrix, which has gained significant attention from researchers and has applications in various fields, like sensor technology, optics, and biomedicine. These modifications can confer chemical specificity and enhanced sensitivity for detecting ultra-low concentration molecules in applications based on SERS or SPR spectroscopy [5-8]. Manufacturing metal nanostructures with superior SERS performances is a major priority for sensing and analysis applications [9]. SERS sensors depend on the Plasmonic features of transition and noble metals. This dependence has been extensively utilized to increase Raman signals as the SPR features of nearby nanostructures are significantly influenced by the coupling effect and inter-particle regions generated by nanostructures of specific shape, size, and composition integrated onto a substrate that is utilized as an analytical tool [7, 10-13]. In summary, it represents a susceptible technology that detects small molecules due to the main advantage of amplifying Raman signals at hotspot regions compared to standard Raman scattering for molecular detection, such as explosives, environmental pollutants, drugs, and pesticides [14, 15]. For a long time, nanostructures of gold (Au) and silver (Ag) have been recognized as ideal metals for SERS applications due to their strong Plasmonic properties [16, 17]. However, Au and Ag's high cost and low stability under certain conditions have motivated researchers to explore alternative metals [18, 19]. Copper (Cu) and palladium (Pd), for instance, have attracted considerable attention and have emerged as promising metals for SERS because of their low cost, equivalent conductivity, and Plasmonic properties compared to Au and Ag nanostructures [20, 21]. Cu, naturally available and inexpensive, exhibits strong and tunable Localized Surface Plasmon Resonance (LSPR) from UV-VIS to IR region. Furthermore, due to its interesting physical and chemical characteristics, Cu shows outstanding catalytic performance in various reactions. Combined with light-harvesting capability and catalytic function, Plasmonic Cu is a promising platform for effective light-driven chemical reactions [22]. The nanosized Copper requires large surface activation energy, resulting in unique features, including a low melting point, robust magnetism and light absorption, and firmness, in addition to a high fraction of surface area, optical properties, antimicrobial activity, and electronic properties and can be easily functionalized [23-25]. Furthermore, palladium exhibits strong plasmonic effects and excellent surface stability, and it can be utilized sufficiently in electrochemistry as a catalyst [11, 26]. Pd nanostructures are advantageous owing to their significant adaptability in terms of reactivity, SPR, which is an essential and valuable feature in sensing, chemo-optical transducers, Plasmonic wave guiding, and the field of SERS [21, 27, 28]. This investigation highlighted the utilization of low-cost, high-SERS-performance metallic nanostructures for environmental detection applications. CuNWs and PdNPs as SERS emphasize the Plasmonic amplification effect as an analytical tool for detecting $NaNO_2$ molecules. Moreover, this work discusses the synthesis method, characterization techniques, and optimization strategy employed to enhance the SERS performance of the Cu/PS and Pd/PS nanostructures. The comparison between the two sensors is discussed based on each sensor's deposition and sensing mechanisms.

2. Experimental Procedure

2.1 Chemicals

Hydrofluoric acid (HF) (C.D.H., England 48%) and high purity ethanol (C_2H_5OH) (Sigma-Aldrich, 99.8%, Germany) were mixed in a ratio of (1:1) (HF: Ethanol) to prepare the required (24%) concentration of HF that required for the fabrication process of PS Immersion plating method employed copper sulfate pentahydrate ($CuSO_4.5H_2O$), and palladium chloride ($PdCl_2$) solutions. $NaNO_2$ was utilized as the analytical solution at concentrations of (5×10^{-1}, 5×10^{-6}) M. All solutions were prepared and dissolved in distilled water. All chemicals were utilized as obtained, with no additional purification.

2.2 Fabrication of Porous Silicon

One mirror side, n-type Silicon (Si) wafer with (100) orientation, (10) Ω.cm, resistivity, and (625) µm thickness was employed in this work. Si wafer has been chopped into (1.5x1.5) cm^2 pieces. These pieces were weighed and immersed in a (1:10) (HF: ethanol) mixture for 10 min, under shaking conditions to remove the SiO_2 layer. The pieces were cleaned with ethanol, then washed with distilled water to remove HF residue, and dried in the air for several minutes. Finally, they were stored in plastic containers full of methanol to maintain their cleanliness and

readiness for the Photo-Electro-Chemical-Etching process (PECE). PECE is a well-known process for the fabrication of PS where the electrochemical and photochemical etching methods provide a combination of the material interaction with HF acid through light and current density, where the illumination of laser light on the Si electrode significantly modifies PS properties [29]. The etching process was conducted at room temperature in a specially designed Teflon cell filled with a (1:1) mix of 24% HF acid and Ethanol solution. The set-up illustrated in **Fig. 1** below consists of (DC) power supply as a current source, Pt. ring as the cathode, Si substrate as the anode, Avometer, Teflon etching cell, and red laser diode of wavelength 630 nm with a specified output power density of about (30) mW/cm^2 as the light source that illuminated about 1 cm^2 of Si area. The etching process occurred with fixed parameters of 20 mA/cm^2 current density and 30 min etching time.

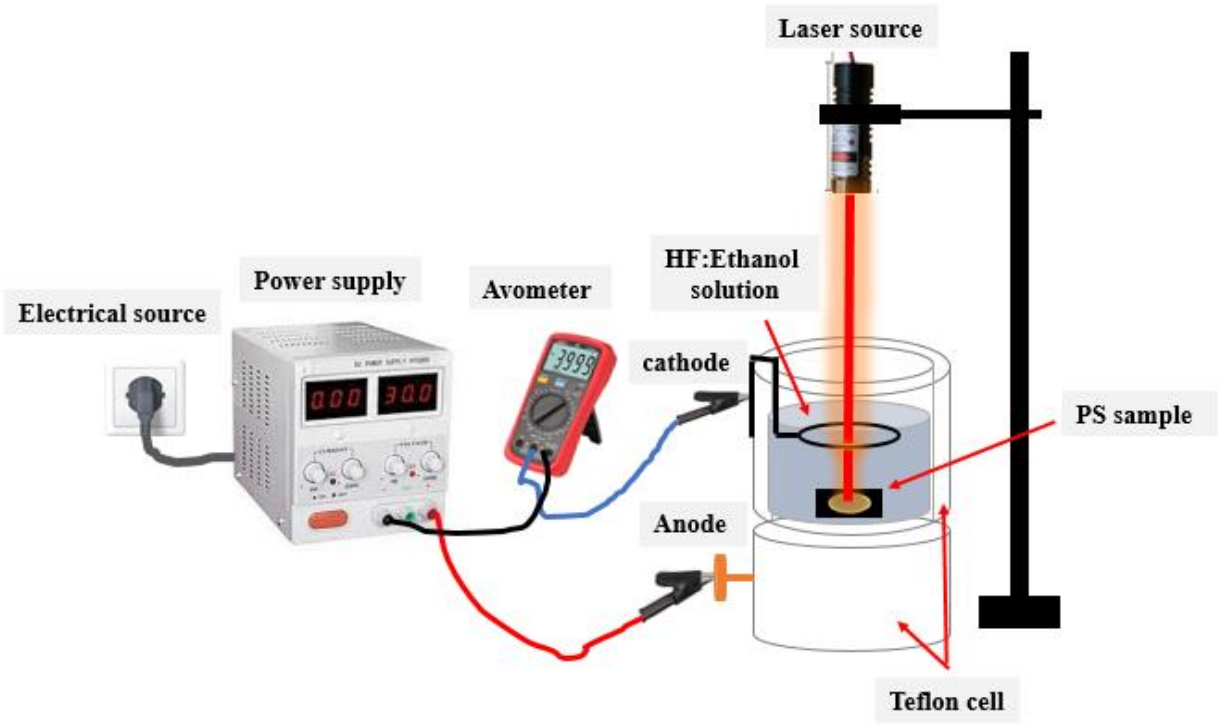

Figure 1: schematic diagram of the experimental set-up of the PECE system.

In the PECE process, laser light supplies the necessary holes in the illuminated area of the Si wafer to start the etching process. When the n-type Si wafer is immersed in the HF acid, its surface becomes saturated with hydrogen (H) atoms, making it inert to further HF acid attacks due to the similar electronegativity of H and Si. Upon illumination with laser light, the Si wafer absorbs the light, creating electron-hole pairs to generate an internal field and a depletion layer in the illuminated area, driving holes to the surface of the Si wafer. These photo-generated holes facilitate the formation of silicon-Floride (Si-F) bonds by replacing H atoms with F atoms on the silicon surface. The polarization of the bonded F atoms leads to removing Si atoms, creating tips that change the surface geometry, increase the surface irregularities, and alter the electric field distribution. Conversely, an etching current density flows from the back side of the wafer through the solution, completing the electrical circuit and enhancing the etching process. As a result, the surface is reconstructed with various probes and columns forming PS [30-32]. The chemical pathway of PS fabrication is illustrated in **Fig. 2** and explained by the following Eq. (1) [3, 33]:

$$Si + 6HF \longrightarrow H_2SiF_6 + 4H + + 4e^- \quad (1)$$

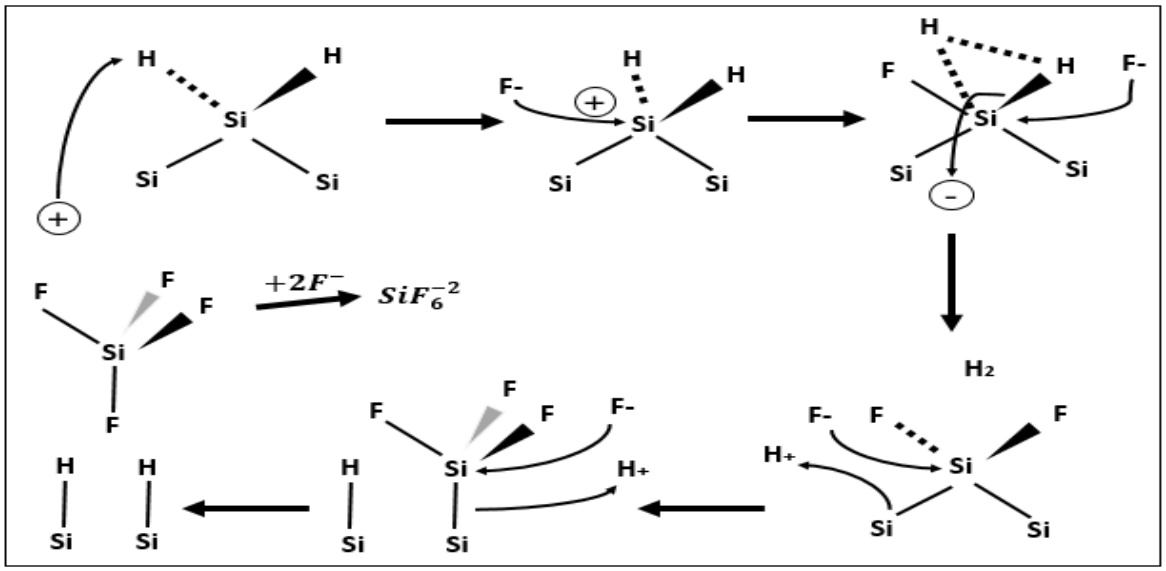

Figure 2: The schematic diagram illustrates the etching mechanism during the PS fabrication process [34].

2.3 Fabrication of Cu /PS and Pd/PS SERS sensors:

Immersion solutions were separately prepared with a concentration of (0.025) M for each. The blue-colored Cu immersion solution was prepared by dissolving $CuSO_4.5H_2O$ powder in distilled water through continuous stirring by a magnetic stirrer for about 15 minutes at room temperature to achieve a complete dissolving process. For the brown Pd immersion solution, $PdCl_2$ powder was dissolved in distilled water mixed with a few drops of 35% concentration HCL acid and heated to 70°C while continuously stirring with a magnetic stirrer for about 30 minutes. To achieve complete dissolving of $PdCl_2$ powder because it is incapable of dissolving entirely in distilled water compared to copper. The required concentrations of these solutions were calculated using the following Eq. (2) [13, 35]:

$$molarity = \frac{W}{MW/V} \qquad (2)$$

W: represents the $CuSO_4.5H_2O$ and $PdCl_2$ weight in (g), MW: refers to molarity weights of $CuSO_4.5H_2O$ and $PdCl_2$, which are ~ 249.72, and 177.32 (g/mole) respectively. V refers to the volume of the dissolved solution. Cu/PS and Pd/PS SERS substrates were fabricated due to the experimental steps illustrated in **Fig. 3** by dipping PS samples in Cu and Pd solutions using an immersion plating process for 30 minutes at room temperature. The immersion plating process is a facile and more economical method than other metal deposition techniques like electrodeposition, inkjet printing, and vapor deposition, where dipping PS in solvents with metal ions will lead to immediate deposition of the metal [36]. The Plasmonic nanostructures are formed at room temperature due to the ion-reduction process [37]. Where the deposition process involved the conversion of copper ions (Cu^{2+}) and palladium ions (Pd^{2+}) to positively charge metallic nanostructures deposited on the PS surface through the gain of electrons (e^-) during the adherence process. In other words, it signifies the reduction of positively charged Copper and palladium ions to neutral metals, leading to the deposition of Cu and Pd on the surface of PS [38, 35]. Regarding the reduction process that describes the interaction between metallic nano-solutions and the PS surface, the following Eq. (3) and (4) explain the reduction processes of Cu and Pd immersion solutions on the PS surface [34, 39]:

$$\boldsymbol{Cu^{2+} + 2e^- \longrightarrow Cu} \qquad (3)$$

$$\boldsymbol{Pb^{2+} + 2e^- \longrightarrow Pb} \qquad (4)$$

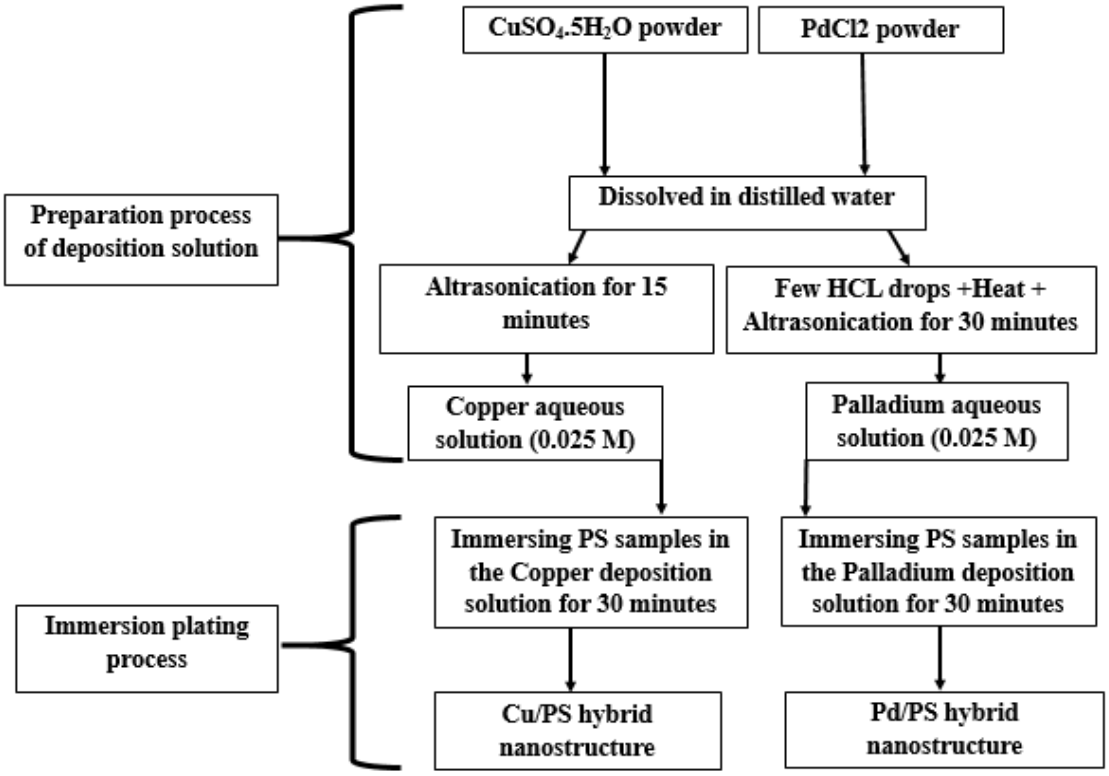

Figure 3: The experimental flow chart of the Cu/PS and Pd/PS SERS substrates fabrication process.

2.4 Instrumentation and data analysis

The morphology and structure of the bare PS, Cu/PS, and Pd/PS SERS sensors were characterized via Field Emission Scanning Electron Microscopy (FESEM) by utilizing the Inspect F50 device. X-ray diffraction (XRD) was characterized by Aeris – Malvern Panalytical diffractometer operating with monochromatized CuK radiation of wavelength (0.154) nm, and Energy Dispersive X-ray Spectroscopy (EDX) using Axia ChemiSEM device. The pore dimensions of bare PS and the sizes of CuNWs and PdNPs were calculated using the image j program. Evaluating the performance and sensing characteristics of Raman and SERS sensors was conducted using the 532 nm pre-configured Raman spectrometer system. The measuring and recording process was conducted at room temperature. The enhancement factor (EF) of Raman peak intensity was calculated using Eq. (5) considering the Raman peak of the sodium nitrite molecule [3]:

$$EF = \frac{I_{SERS} X C_R}{I_R X C_{SERS}} \qquad (5)$$

IR and ISERS refer to the corresponding counterpart intensities of regular Raman and SERS. CR and CSERS correspondingly represent the probe's regular Raman and SERS concentrations.

3. Results and Discussion

3.1 Morphological characterization of bare PS, Cu/PS, and Pd/PS SERS structures:

According to **Fig. 4,** the FESEM images of photoelectrochemically etched PS described the formation of a pore-like structure with different pore diameter dimensions. At 5 µm magnification, the PS surface, after 30 minutes of etching time with laser and electricity, exhibits a distinctive pattern of square-shaped pores arranged in a regular and well-defined manner. These square-shaped pores are uniformly distributed across the surface, forming a structured array. The edges of the squares are straight and form right angles, resulting in a characteristic grid-like appearance. Also, the PS surface displays pore size distribution that varies from large to small pore sizes, creating a gradient of pore properties. These results mean that the pores' size, depth, or density gradually changes across the surface because the 30 min etching time was enough to etch the silicon surface repeatedly, resulting in

overlapping in the opening of the pores, graded pores structures leading to increased surface area of the porous layer. Combining square-shaped pores and graded pore distribution gives the surface a unique and visually appealing structure. The square pores provide a regular and organized pattern, while the graded pore distribution adds depth and complexity to the surface structure. This graded distribution allows for developing surface properties, such as surface area, pore connectivity, and optical properties, over different material regions that can be adjusted to suit specific application requirements. The interesting finding was that the sensitivity of PS relies on the morphological properties of pores, including pores diameter and homogeneity, surface uniformity, and porous layer thickness [40]. The formation of pores on the silicon surface increases the coating rate, consequently considering the chemically active area. This type of PS surface offers potential advantages in sensing fields, where precise control over pore size and distribution is crucial for optimizing device performance [41].

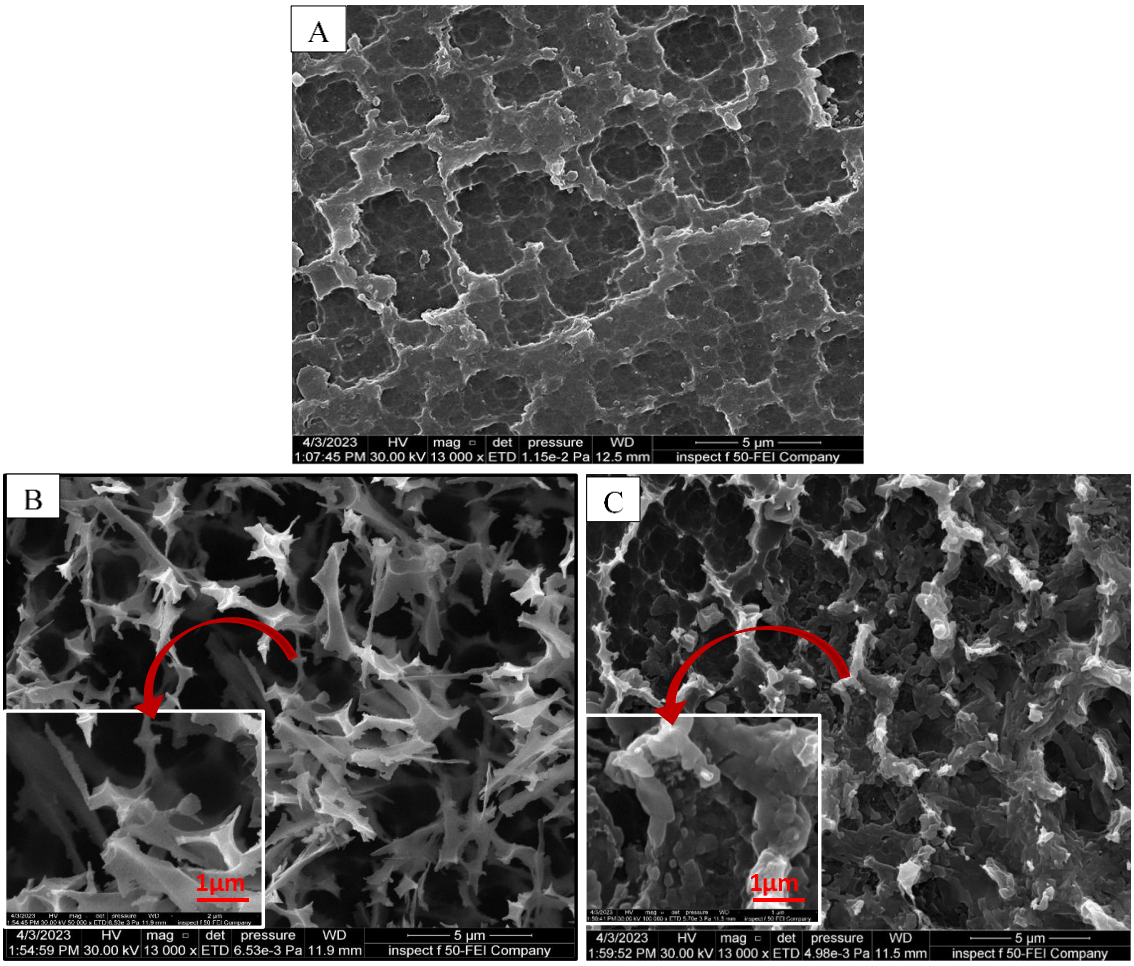

Figure 4: FESEM images with different magnifications of **a**) bare PS **b**) Cu/PS **c**) Pd/PS SERS substrate structures.

Figs. 4b and **4c** show the SEM top view of Cu/PS and Pd/PS structures, respectively. Understanding the quality of structure and adherence is essential for optimizing the performance of PS-based devices in various applications, varying from sensors to energy storage systems. The PS surface acts as a captivating surface for the adhesion of these nanostructures. CuNWs are deposited on the PS layer, creating, and appealing an indicative, significant pattern of thorn-like nanowire structures resembling an artistic representation of Cu nanostructures. The resulting nanowire morphology presents a captivating harmony of sharp edges, irregular shapes, and interlocking structures. CuNWs are characterized by their elongated and one-dimensional morphology, aligning along the pores of the silicon matrix, forming a continuous and interconnected network. This structural configuration enhances the mechanical stability of the modified surface. The chemical displacement deposition of Cu on PS exhibited Cu nanowires distributed on the porous layer with high adhesion and simple control, and it requires no special

equipment, which agrees with [42]. For PdNPs deposited onto the surface of PS, as illustrated in **Fig. 4c**, PdNPs within the solution selectively and directly adhere to the exposed surfaces and walls of the sophisticated network of pores on the PS architecture, creating a thin, conformal, and continuous film of palladium layer. The formed thin covering layer of PdNPs follows the shape of the pores without blocking or compromising the structural reliability. PdNPs flawlessly envelop the porous matrix's framework while preserving the original surface's distinct morphology, allowing continued interaction with the surrounding environment. For both Cu/PS and Pd/PS SERS structures, the interaction between the metals and PS substrate forms a harmonious union, where a combination of electrostatic forces and chemical bonding control the deposition process, allowing for a more adaptable conformal coverage [43]. Comparing the two distinct metals reveals significant differences in aggregation and adherence mechanisms. Where CuNWs exhibited a more irregular arrangement, displaying a tendency for aggregation. PdNPs are typically characterized by a continuous and uniform distribution of nanostructures, forming a robust and closely packed monolayer on the porous silicon surface. In other words, CuNWs exhibited weaker adherence, relying more on van der Waals forces, leading to a comparatively less stable configuration. At the same time, PdNP nanostructures adhere strongly through a combination of electrostatic and chemical bonds, ensuring long-term stability. This structural difference is attributed to their physical and chemical surface properties, such as the metals' inherent nature and interaction with porous silicon. PS was generated with an average pore diameter of (0.973) µm. In contrast, CuNWs and PdNPs were generated with an average particle size of (0.278) µm and (0.302) µm, respectively, as shown in **Fig. 5a, 5b**, and **5c**. The above results indicate that the sizes of CuNWs and PdNPs could be considered vital elements of the PS structure properties (pores construction and surface roughness).

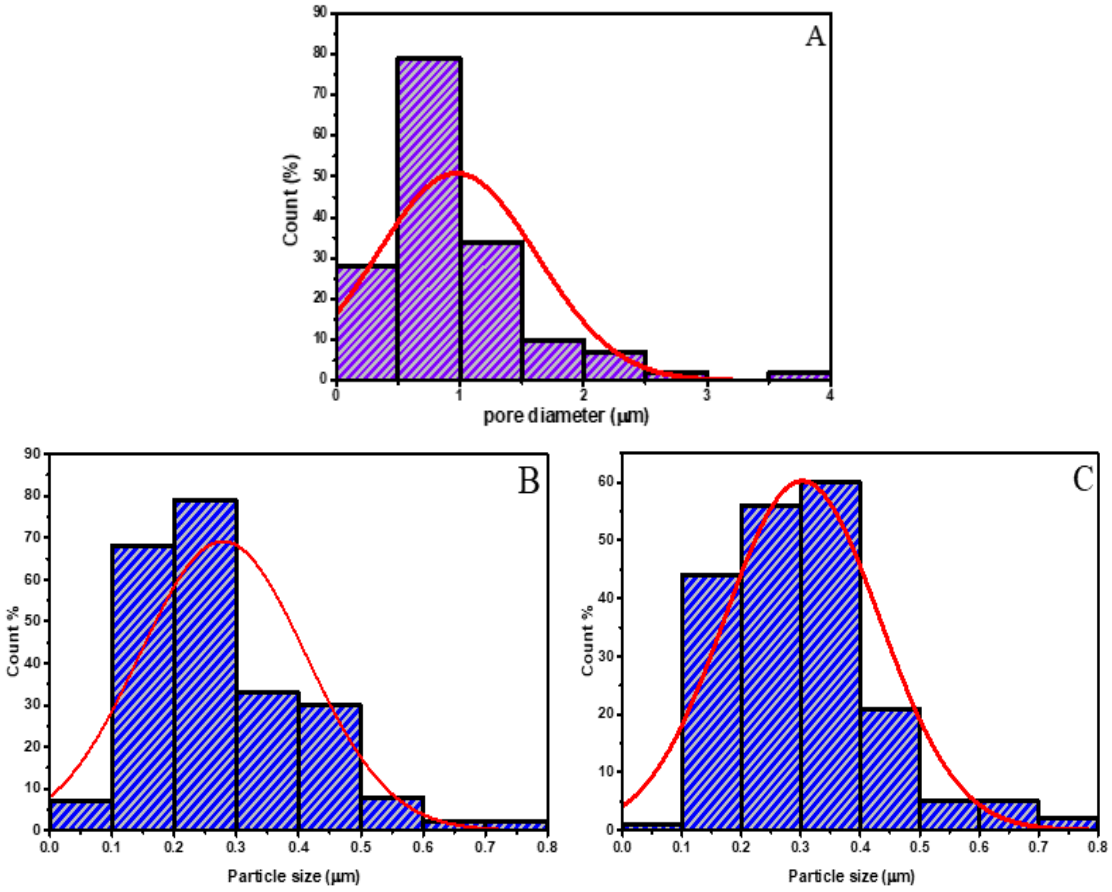

Figure 5: Statistical size histograms of **a**) PS pores, **b**) CuNWs, and **c**) PdNPs.

XRD analysis was performed to determine the structure and crystallographic phases of the samples. As revealed in **Fig. 6a, 6b,** and **6c**, the XRD patterns showed different diffraction peaks; for PS, a single diffraction peak at 33.38˚ was observed, proving its FCC structure. Furthermore, CuNWs presented diffraction peaks at 43.2˚ and 51.6˚, While for PdNPs, the XRD patterns showed diffraction peaks located at 40.45˚, 46.7˚, and 68.5˚. For

calculation requirements, the characteristics reflect the face-centered structure (FCC). CuNWs and PdNPs are comparable to the standard JCPDS files No. 00-004-0836 and 87-0641 [2, 25]. The metallic nanostructure sizes (D) were calculated using Scherer's equation [44, 45], while the specific surface area (SSA) was calculated using the following Eq. (6) and (7) [3]:

$$\boldsymbol{D} = \frac{\boldsymbol{0.9\,k}}{\boldsymbol{\beta\,cos\,\theta}} \qquad (6)$$

$$\boldsymbol{S.S.A.} = \frac{\boldsymbol{6000}}{\boldsymbol{D{*}\rho}} \qquad (7)$$

D and ρ represent the grain size of Cu and Pd nanostructures, respectively. The density of copper and palladium nanostructures (8.96) and (12.007) gm/cm^3 respectively. The data of XRD measurements concerning the bare PS, Cu/PS, and Pd/PS substrates are illustrated in Table 1.

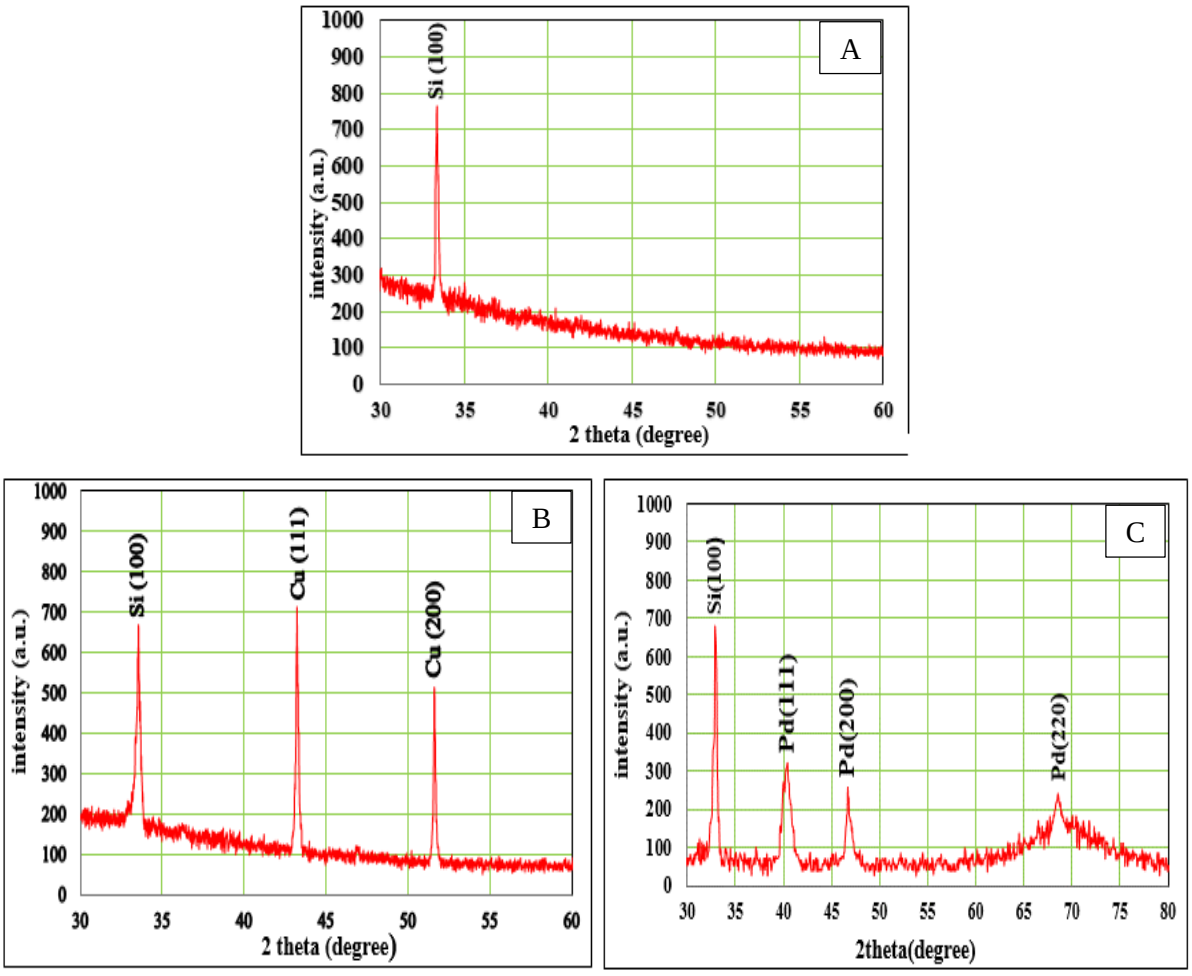

Figure 6: XRD patterns of **A**) bare PS B**b**) Cu/PS **C**) Pd/PS SERS substrates.

The EDX mapping of the SERS sensors with CuNWs and PdNPs deposited on the PS surface is demonstrated in **Fig. 7A,** and **7B**. The DEX analysis has verified the presence of silicon, Copper, and Palladium on the SERS sensors. The substrate is the silicon source. Due to the values illustrated in **Fig. 7C**, the CuNWs showed higher deposition rates than PdNPs.

Table 1: XRD data of bare PS, Cu/PS, and Pd/PS SERS substrates.

Sample	**Bare PS**	**Cu/PS**			**Pd/PS**			
Element	Si	Si	Cu	Cu	Si	Pd	Pd	Pd
Plane	(100)	(100)	(111)	(200)	(100)	(111)	(200)	(220)
2Θ (˚)	33.38	33.5	43.2	51.6	32.95	40.45	46.7	68.5
FWHM (rad.)	0.0042	0.0068	0.0033	0.0031	0.0079	0.0226	0.013	0.0514
Grain size(nm)	-	-	45.22	46.69	-	6.54	11.6	3.27
S.S.A. (m^2/gm)	-	-	14.8	14.34	-	76.3	43.02	152.6

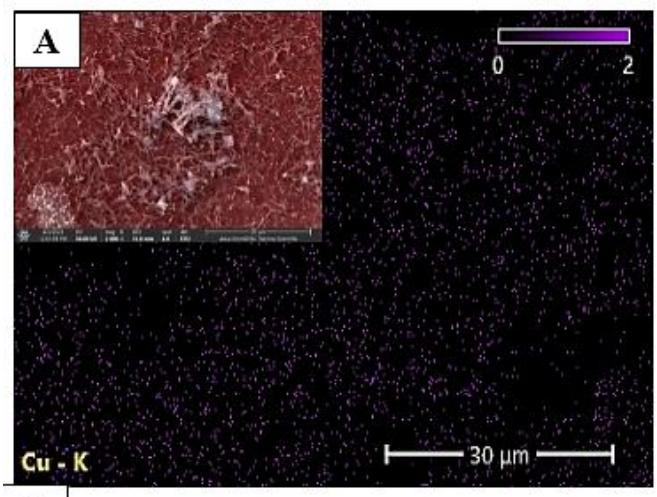

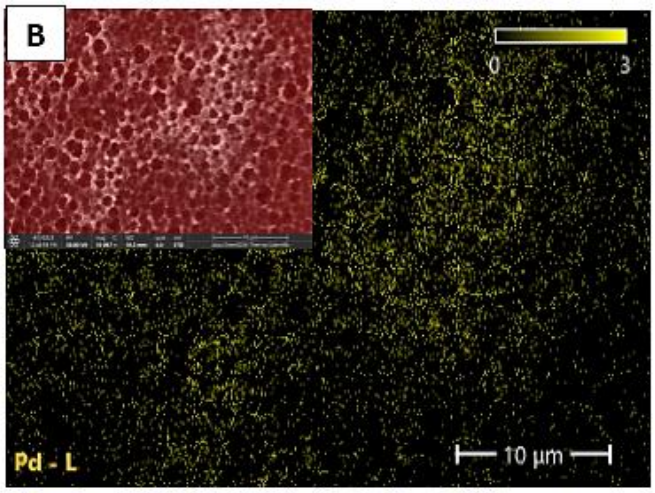

C

Element	Atomic %	Weight %
Si	49.3	48.3
O	14.1	11.6
Cu	36.6	40.1

Element	Atomic %	Weight %
Si	51.6	54.3
O	9.2	9.1
Pd	39.2	36.6

Figure 7: Energy dispersive X-ray (EDX) mapping of **A**) CuNWs, **B**) PdNPs, and **C**) percentage values of CuNWs and PdNPs on PS surface.

3.2 Sensing performance of bare PS, Cu/PS, and Pd/PS SERS sensors

The sensing performance of Raman and SERS sensors for $NaNO_2$ was examined as presented in **Fig. 8a, 8b,** and **8c**. The Raman spectra of $NaNO_2$ for bare PS were initially investigated at a high concentration of about 0.5 M. In contrast, for the Cu/PS and Pd/PS sensors, the SERS spectra were examined at a low concentration of (5×10^{-6}) M.

$NaNO_2$ solution, even with high concentration, has an extremely weak Raman response for bare PS sensors. For Cu/PS and Pd/PS SERS sensors, the Raman peak at extremely low nitrite concentration was enhanced intensely by incorporating the CuNWs and PdNPs on the surface of PS due to the SERS effect. The significant Raman spectrum of $NaNO_2$ for bare PS, Cu/PS, and Pd/PS SERS sensors is ascribed at specific vibrational modes of the following peaks demonstrated in Table 2. These peaks are Raman fingerprints of sodium nitrite [46-48].

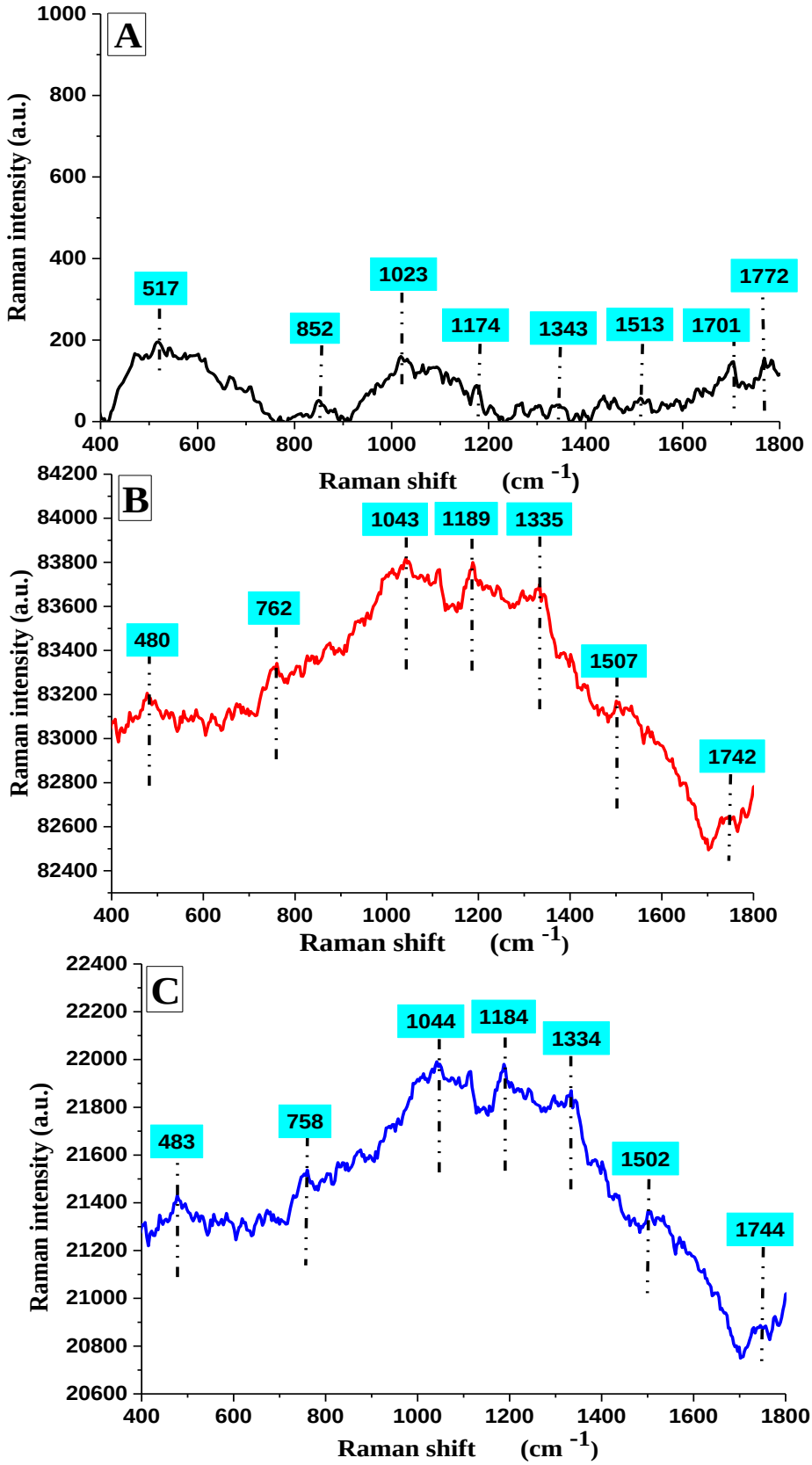

Figure 8: Raman spectra of $NaNO_2$ for **A**) bare PS **B**) Cu/PS **C**) Pd/PS SERS sensors.

Table 2: Raman spectra of $NaNO_2$ at concentrations of $5x10^{-1}$ M for bare PS sensor, $5x10^{-6}$ M for Cu/PS and Pd/PS SERS sensors.

At concentration = $5x10^{-1}$ M		**At concentration = $5x10^{-6}$ M**			
Bare PS sensor		**Cu/PS SERS sensor**		**Pd/PS SERS sensor**	
Raman shift (cm^{-1})	**Vibrational modes**	**Raman shift (cm^{-1})**	**Vibrational modes**	**Raman shift (cm^{-1})**	**Vibrational modes**
517	COO bend + CH_2 bend	480	COO bend+ CH_2 bend	483	COO end+ CH_2 bend
852	C=C stretch in ring	762	O-H out of plane	758	C=O
1023	C-O-H bend	1043	C-CH_3 stretch	1044	C-CH_3 stretch
1174	C-O-C stretch	1189	C-O-C stretch	1184	C-O-C stretch
1343, 1513	C-H bend	1335,1507	C-H bend	1334,1502	C-H bend
1701, 1772	C=O	1742	C=O	1744	C=O

According to Table 2 above, the SERS spectrum signifies the main modes of sodium nitrite when compared with the Raman spectrum of bare PS. The extremely weak signal of the Raman spectrum can be assigned to the infiltration of the $NaNO_2$ analyte within the PS substrate that conveys the analyte far from the excitation. Hence, the light spot was unclarified in this effect. The extremely strong SERS spectra of $NaNO_2$ absorbed on the Cu /PS and Pd/PS SERS-active substrates can be attributed to hot spot regions surrounded by CuNWs and PdNPs and to the precise surface area. An effective energy transmission occurs between the metallic nanostructures and the nitrite within the regions of a hot spot, improving the sensors' detection effectiveness and increasing the Raman signal. Overall, the excellent activity of the CuNWs and PdNPs deposited on the PS substrate signifies the surface enhancement performance of Cu/PS and Pd/PS SERS sensors. The unique morphology of PS decorated by CuNWs and PdNPs with hot spot regions generated significantly improves the local electromagnetic (EM) field near the metal nanostructures. It affords a simple, fast, and susceptible detection process by concentrating light into small volumes, thereby using the field enhancement characteristics of metal nanostructure to increase the typically weak Raman scattering signals [9, 49]. Top of Form

Furthermore, Cu/PS and Pd/PS nitrite sensors showed stable performance without any saturation effects, leading to an exceptional increase in EF with decreasing nitrite concentration by strengthening the SERS signal. The most vital parameter that evaluates the activity and efficiency of the sensors is the enhancement factor (EF), estimated from equation (5). The highest EF achieved from the Cu/PS sensor was ($0.43X10^8$) while for the Pd/PS sensor, it was ($0.11X10^8$) revealing the enhancement ability of the Cu/PS SERS sensor higher than that obtained in the case of the P/PS SERS sensor. Table 3 below illustrates this work's main results and applications compared with other studies concerning metal plasmonic materials deposited on PS via different deposition methods, such as SERS sensors.

Table 3: Different metallic nanostructures deposited on porous silicon via different deposition methods as SERS substrates for different sensing applications.

Metal	**structure**	**Deposition method**	**Main results**	**Application**	**Ref.**
Cu Pd	Nanowires Nanoparticles	Immersion Plating (Chemical Reduction)	The two separate metals display distinctive Plasmonic characteristics appropriate for boosting Raman signals as SERS Plasmonic materials. EF(CuNWs) =0.48 $x10^6$ EF(PdNPs) =0.11$x10^6$	Environmental detection ($NaNO_2$)	This work
Au	Nanoparticles	Immersion Plating	The sensor activity is dependent on the ratio of hot spots and the exact surface area of Au nanoparticles.	Chlorpyrifos Pesticides detection	[33]

		(Chemical Reduction)	EF=8.8 x10^5		
Ag	Nanoparticles	Pulsed Laser Deposition (PLD)	Combining the enormous surface-to-volume ratio of Si NW arrays with the plasmonic characteristics of silver nanoparticles produced a 3D structure ideal for highly sensitive surface-boosted Raman scattering. (SERS) applications EF (not calculated)	R6G	[50]
Al	Nanopillars	Evaporation	The configuration of precise Al/Si nanopillars developed on a large-area Si wafer caused an excellent homogeneity of the SERS signal throughout the whole wafer. EF= $1.5 \times 10^7 - 2.5 \times 10^7$	Chemical detection (Thiophenol molecules.)	[51]
Au	Nanoparticles	Physical Vapor Deposition (P.V.D.)	The homogeneous distribution of SERS-active 'hotspots' on the Au/Si surface leads to excellent repeatability when detecting p-MBA at 40 separates, randomly placed on a single substrate. EF=10^8	Chemical analysis p-mercaptobenzoic acid (p-MBA)	[52]
Au	Nano-cylinders	UV-Nanoimprint Lithography (UV-NIL)	Gold nanocylinders (GNCs) proved to be extremely sensitive and selective sensing surfaces. EF=3.7×10^7	Biosensing (Cysteamine, D.D.T., and Biotin)	[53]

4. Conclusions

A simple and successful approach was employed to fabricate Cu/PS and Pd/PS SERS substrates as nitrite sensors. CuNWs and PdNPs revealed significant differences in structural properties and adherence mechanisms relying on a combination of electrostatic forces and chemical bonding for adhesion, allowing for more adaptable and conformal coverage. This study suggested that the specific reduction mechanism can depend on various factors, including the composition of the CuNWs and PdNPs, the features of the PS surface, and the experimental conditions. The two distinct metals exhibited unique Plasmonic properties suitable for enhancing Raman signals as SERS Plasmonic materials. The Raman signal for the nanocrystalline size of PS improved with CuNWs and PdNPs intensity depending on the geometric shape and the distribution density of nanomaterials hotspot region between them. In conclusion, the findings confirmed the potential of CuNWs and PdNPs as promising characteristics of Plasmonic materials for SERS applications. However, further investigation revealed Copper as the ideal alternative for achieving optimal SERS performance. Copper emerged as the superior metal due to several critical factors regarding its strong Plasmonic properties, higher surface roughness providing more active sites for analyte adsorption, and better chemical stability under SERS conditions, leading to improved performance by enhancing SERS signal four times higher compared to Pd/PS SERS sensor. Additionally, Copper is a more viable option for large-scale SERS environmental sensing applications owing to its low cost and availability.

Conflict of Interest

The authors declare that they have no conflict of interest.

References

[1] R. Moretta, L. De Stefano, M. Terracciano, and I. Rea, "Porous silicon optical devices: recent advances in biosensing applications". *Sensors*, Vol. 21, no. 4, pp.1336, 2021.

[2] M. Khan, G. H. Albalawi, M. R. Shaik, M. Khan, *et al.*, "Miswak mediated green synthesized palladium

nanoparticles as effective catalysts for the Suzuki coupling reactions in aqueous media". *Journal of Saudi Chemical Society*, vol. 21, no. 4, pp. 450–457, 2017.

[3] D. S. Jubair, A. M. Alwan, and Hamoudi, W. K. "Sensing Performance of Mono and Bimetallic Nano Photonics Surface Enhanced Raman Scattering (SERS) Devices". *Engineering and Technology Journal*, vol. 39. no.7, pp.1174-1184, 2021.

[4] M. Moaied, S. Palomba, and K. Ostrikov, "Longitudinal quantum plasmons in copper, gold, and silver". *arXiv preprint arXiv*, pp.1708.04059, 2017.

[5] A. A. Yousif, A. M. Alwan, and H. R. Abed, "Optimizing of macro porous silicon morphology for creation of SnO2/CuO nanostructures". AIP Publishing in AIP Conference Proceedings, Vol. 2213, no. 1, 25/03/ 2020.

[6] A. M. Alwan, D. A. Hashim, and M. F. Jawad, "Optimizing of porous silicon alloying process with bimetallic nanostructures". *Gold Bulletin*, vol.51, no.4, pp.175-184, 2018.

[7] A. M. Alwan, M. S. Mohammed, and R. M. Shehab, "Optimization of an ultra-sensitive Ag core-Au shell nanoparticle/Si Surface-enhanced Raman scattering (SERS) sensor". AIP Publishing in AIP Conference Proceedings, vol. 2307, no. 1, 15/12/2020.

[8] M. Kahraman, E. R. Mullen, A. Korkmaz, and S. Wachsmann-Hogiu, "Fundamentals and applications of SERS-based bioanalytical sensing. *Nanophotonics*, vol. 6, no.5, pp.831-852, 2017.

[9] H. Wei, and H. Xu, "Hot spots in different metal nanostructures for plasmon-enhanced Raman spectroscopy" *Nanoscale*, vol. 5, no.22 , pp.10794-10805, 2013.

[10] A. M. Al-Syadi, M. Faisal, F. A. Harraz, M. Jalalah, *et al.*, "Immersion-plated palladium nanoparticles onto meso-porous silicon layer as novel SERS substrate for sensitive detection of imidacloprid pesticide. *Scientific Reports*, vol.11, no.1, pp.9174, 2021.

[11] S. F. Abbas, A. J. Hadier, Sh. Al-Musawi, and B. A. Taha, "Synthesis of High-Performance Antibacterial Magnesium Oxide Nanostructures through Laser Ablation ",*Journal of Applied Sciences and Nanotechnology*, Vol. 4, no. 1, pp.35-65, 2024.

[12] W. H. Ali, A. B. Dheyab, A. M. Alwan,, and Z. S. Abber, "Study the role of mud-like Psi morphologies on the performance of AuNPS SERS sensor for efficient detection of amoxicillin", AIP Publishing, in *AIP Conference Proceedings* ,vol. 2290, no. 1, 4/12/2020.

[13] A. M. Alwan, and I. A. Naseef, "Optimization of photoluminescence properties of Porous silicon by adding gold nanoparticles". *Iraqi Journal of Science*, vol.58, no.1 A , pp. 53-62, 2017.

[14] M. Q. Zayer., and A. M. Alwan, "Active control of silver nanostructure aggregates for ultrahigh sensitive SERS detection of organic molecules: single molecule approach", *International Journal of Nanoelectronics and Materials*, vol.12, no.1, pp. 55-66, 2019.

[15] L. A. Wali, K. K. Hasan, and A. M. Alwan, "Rapid and highly efficient detection of ultra-low concentration of penicillin G by gold nanoparticles/porous silicon SERS active substrate". *Spectrochimica Acta Part A: Molecular and Biomolecular Spectroscopy*, vol.206, pp.31-36, 2019.

[16] R. B. Rashid, A. M. Alwan, and M. S. Mohammed, "Room Temperature 2-Fold Morphology Porous Silicon Impedance Matching Pesticide Sensor", *Journal of Applied Sciences and Nanotechnology*, Vol. 3, no.1 ,2023.

[17] P. A. Atanasov, N. N. Nedyalkov, N. Fukata,, *et al.*, "Surface-enhanced Raman spectroscopy (SERS) of neonicotinoid insecticide thiacloprid assisted by silver and gold nanostructures". *Applied Spectroscopy*, vol. 74, no.3, pp.357-364, 2020.

[18] G. V. Naik, V. M. Shalaev, and A. Boltasseva, "Alternative plasmonic materials: beyond gold and silver. *Advanced Materials*, vol.25, no.24, pp.3264-3294, 2013.

[19] A. Sultangaziyev, A. Ilyas, A. Dyussupova, and R. Bukasov, "Trends in application of SERS substrates beyond Ag and Au, and their role in bioanalysis. *Biosensors*, vol.12, no.11, pp.967, 2022.

[20] A. Kumar, M. M. Mohammadi, and M. T. Swihart, "Synthesis, growth mechanisms, and applications of palladium-based nanowires and other one-dimensional nanostructures. *Nanoscale*, vol.11, no.41, pp.19058-19085, 2019.

[21]. S. F. Abbas, A. J. Haider, Sh. Al-Musawi, and B. A. Taha, "Synthesis of High-Performance Antibacterial Magnesium Oxide Nanostructures through Laser Ablation", *Journal of Applied Sciences and Nanotechnology*, vol. 4, no. 1, 2024.

[22] Y. Xin, K. Yu, L. Zhang, Y. Yang, H. Yuan, *et al.*, "Copper-based plasmonic catalysis: recent advances and future perspectives". *Advanced Materials*, vol.33, no.32, pp.2008145, 2021.

[23] H. Khalid, S. Shamaila, N. Zafar, and S. Shahzadi, "Synthesis of copper nanoparticles by chemical reduction

method". *Sci. Int*, vol.27, no. 4, pp.3085-3088, 2015.
[24] S. Shahsavari, S. Hadian-Ghazvini, F. H. Saboor, and I.M. Oskouie, "Ligand functionalized copper nanoclusters for versatile applications in catalysis, sensing, bioimaging, and optoelectronics". *Materials Chemistry Frontiers*, vol.3, no.11, pp.2326-2356, 2019.
[25] G. B. Hong, J. F. Wang, K. J. Chuang, H.Y. Cheng, *et al.*, "Preparing copper nanoparticles and flexible copper conductive sheets". *Nanomaterials*, vol.12, no.3, pp.360, 2022.
[26] D. Raj, F. Scaglione, and P. Rizzi, "Rapid Fabrication of Fe and Pd Thin Films as SERS-Active Substrates via Dynamic Hydrogen Bubble Template Method". *Nanomaterials*, vol.*13*, no.1, pp.135, 2022.
[27] I. Favier, D. Pla, and M. Gómez, "Palladium nanostructures in polyols: Synthesis, catalytic couplings, and hydrogenations". *Chemical reviews*, vol.120, no.2, pp.1146-1183, 2019.
[28] R. K. Petla, S. Vivekanandhan, *et al.*, "Soybean (Glycine max) leaf extract based green synthesis of palladium nanoparticles", *Journal of Biomaterials and Nanobiotechnology*. Vol. 3, no. 1, pp. 14-19. 2011.
[29]. A. M. Alwan, and R. A. Abbas, "Effects of the porous silicon morphology on the gas sensor performance". *International Journal of Engineering Sciences & Research Technology*, vol.6, no.1, pp.204-217, 2017.
[30] A. G. Cullis, L. TPDJ Canham, and P. D. J. Calcott. "The structural and luminescence properties of porous silicon." *Journal of applied physics*, vol.82, no.3, pp.909-965, 1997.
[31] H. Föll, M. Christophersen, J. Carstensen, and G. Hasse, "Formation and application of porous silicon", *Materials Science and Engineering: R: Reports*, vol.39, no.4, pp.93-141., 2002.
[32] C. Vingoni, and M. Cazzanelli, "Porous Silicon microcavities", Department of physics and Astronomy, university of Pittsburgh, Pittsburgh PA, USA, vol. 2, pp.123-192,2000.
[33] W. K. Hamoudi, A. M. Alwan, and D. Sulaiman, "Efficient fabrication of SERS plasmonics pesticides sensors by pulsed laser etching". AIP Publishing in *AIP Conference Proceedings*, vol. 2372, no.1, 2021.
[34] E. J. Anglin, L. Cheng, W. R. Freeman, and M. J. Sailor, "Porous silicon in drug delivery devices and materials", *Advanced drug delivery reviews*, vol.60, no.11, pp.1266-1277, 2008 .
[35] A. M. Alwan, I. A. Naseef, and A. B. Dheyab, "Well controlling of plasmonic features of gold nanostructures on macro porous silicon substrate by HF acid concentration". *Plasmonics*, vol.13, no.6, pp.2037-2045, 2018.
[36] A. M. Alwan, A. J. Hayder, and A. A. Jabbar, "Study on morphological and structural properties of silver plating on laser etched silicon". *Surface and Coatings Technology*, vol.283, pp.22-28, 2015.
[37] R. A. Shlaga, A. M. Alwan, and M. S. Mohammed, "Novel controlling pathway for metallic nanoparticles by laser assisted ion-reduction process". *Journal of Ovonic Research*, vol.19, no.2, pp.219-230, 2023.
[38] H. Bandarenka, S. Redko, P. Nenzi, and M. Balucani, "Optimization of chemical displacement deposition of copper on porous silicon". *Journal of Nanoscience and Nanotechnology*, vol.12, no.11, pp.8725-8731, 2012.
[39] N. Brahiti, T. Hadjersi, H. Menari, S. Amirouche, and O. El Kechai, "Enhanced photocatalytic degradation of methylene blue by metal-modified silicon nanowires" *Materials Research Bulletin*, vol.62, pp.30-36, 2015.
[40] R. A. Ismail, K. S. Khashan, and A. M. Alwan, "Study of the effect of incorporation of CdS nanoparticles on the porous silicon photodetector", *silicon*, vol. 9, pp.321-326, 2017.
[41] G. Huang, J. Han, Z. Lu, D. Wei, *et al.*, "Ultrastable silicon anode by three-dimensional nanoarchitecture design", *ACS nano*, vol. 14,no.4, pp.4374-4382, 2020.
[42] H. Bandarenka, S. Redko, P. Nenzi, and M. Balucani, "Copper displacement deposition on nanostructured porous silicon". *Nanotech*, vol. 2, pp.269-272, 2011.
[43] J. Borges, and J. F Mano, "Molecular interactions driving the layer-by-layer assembly of multilayers", *Chemical reviews*, vol. 114, no.18, pp.8883-8942, 2014.
[44] J. I. Langford, and A. J. C. Wilson, "Scherrer after sixty years: a survey and some new results in the determination of crystallite size", *Journal of applied crystallography*, vol. 11, no.2, pp.102-113, 1978.
[45]P. Scherrer, "Nachr Ges wiss goettingen", *Math. Phys.* vol.2, pp.98-100, 1918.
[46]J. P. Berumen, E.O. Borunda, A.D. Moller, and R. S. Molina,"A study of the optical properties of semi-organic crystals doped with erbium",2011. [Online] http://cimav.repositorioinstitucional.mx/jspui/handle/1004/977.
[47] S. Boca, D. Regina, A. Pintea, N. Leopold, and S. Astilean, "Designing gold nanoparticle-ensembles as surface enhanced Raman scattering tags inside human retinal cells", *Journal of Nanotechnology*, vol.2012, no.1, pp.961216, 2012.
[48] K. Yuniarto, Y. A. Purwanto, S. Purwanto, B. A. Welt, *et al.*, "Infrared and Raman studies on polylactide acid and polyethylene glycol-400 blend". AIP Publishing in *AIP Conference Proceedings*, vol. 1725, no.1, p.961216, 2016.

[49] M.A. Correa-Duarte, N. Pazos Perez, L. Guerrini, *et al.*, "Boosting the quantitative inorganic surface-enhanced Raman scattering sensing to the limit: the case of nitrite/nitrate detection". *The Journal of Physical Chemistry Letters*, vol.6, no.5, pp.868-874, 2015.

[50] C. D'Andrea, M. J. L. Faro, G. Bertino, P. M. Ossi, *et al*, "Decoration of s"licon nanowires with silver nanoparticles for ultrasensitive surface-enhanced Raman scattering". *Nanotechnology*, vol.27, no.37, pp.375603, 2016.

[51] G. Magno, B. Bélier, and G. Barbillon, "Al/Si nanopillars as very sensitive SERS substrates", *Materials*, vol.11, no.9, pp.1534, 2018.

[52] A. Kamińska, T. Szymborski, T. Jaroch, *et al,* "Gold-capped silicon for ultrasensitive SERS-biosensing: Towards human biofluids analysis", *Materials Science and Engineering: C*, vol.84, pp.208-217, 2018.

[53] M. Cottat, N. Lidgi-Guigui, I. Tijunelyte, *et al.,* "Soft UV nanoimprint lithography-designed highly sensitive substrates for SERS detection", *Nanoscale research letters*, vol. 9, pp.1-6, 2014.